Available online at www.sciencedirect.com
ScienceDirect
Journal of Sound and Vibration 297 (2006) 946–961
JOURNAL OF SOUND AND VIBRATION
www.elsevier.com/locate/jsvi

The control of ground-borne vibrations from railway traffic by means of continuous floating slabs

G. Lombaert*,[1], G. Degrande, B. Vanhauwere, B. Vandeborght, S. François

Department of Civil Engineering, K.U.Leuven, Kasteelpark Arenberg 40, B-3001 Leuven, Belgium

Received 12 April 2005; received in revised form 28 April 2006; accepted 2 May 2006
Available online 18 July 2006

Abstract

This paper deals with the effectiveness of a floating slab track for the control of ground-borne vibrations generated by rail transportation systems. The effectiveness is studied by means of a three-dimensional numerical model for the prediction of railway induced vibrations that fully accounts for the interaction between the train, the track and the soil. The incorporation of a resilient mat in a slab track system results in a resonance phenomenon that is determined by the mass of the slab track and the resilience of the mat. At frequencies higher than the slab resonance frequency, the concrete slab uncouples from the underlying soil and the transfer of vibrations is reduced. The effective reduction in the free field, however, is highly dependent on the dynamic characteristics of the slab and the soil. In the case where the phase velocity of the bending waves in the slab is higher than the phase velocity of the Rayleigh waves in the soil, the radiation of waves into the free field is modified. As a result, the reduction of the free field vibrations depends on the angle between the track and the line between the source on the track and the receiver in the free field. In the case where the phase velocity of the bending waves in the slab is much lower than the phase velocity of the Rayleigh waves, a more uniform reduction of the free field response is obtained.

1. Introduction

Ground-borne vibrations due to railway traffic have become important environmental issues, which are particularly critical when new rail infrastructure is introduced in an existing urban environment [1].

Ground-borne vibrations can be controlled at different levels along the transmission path between the source and the receiver. At the source side, the dynamic vehicle characteristics can be modified, the wheel/rail unevenness can be reduced and resilient elements such as ballast mats or slab mats can be incorporated at different levels in the track structure [2–4] (Fig. 1). This paper concentrates on the effectiveness of floating slab tracks for the control of ground-borne vibrations.

In the case of a floating slab track, the slab rests on a resilient mat. The presence of the resilient mat results in a slab resonance frequency, which should be as low as possible for an effective reduction of the free field

*Corresponding author. Tel.: 32 16 32 17 72; fax: 32 16 32 19 88.
E-mail address: geert.lombaert@bwk.kuleuven.ac.be (G. Lombaert).
[1]Postdoctoral Fellow of the Research Foundation-Flanders (FWO-Vlaanderen).

0022-460X/$ - see front matter © 2006 Elsevier Ltd. All rights reserved.
doi:10.1016/j.jsv.2006.05.013

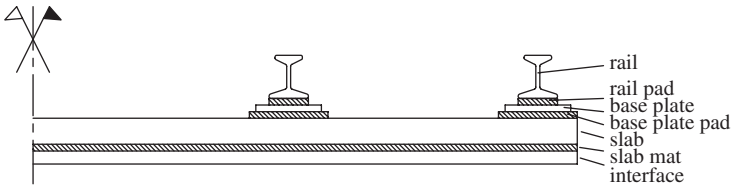

Fig. 1. Transversal section of a slab track.

vibrations. The slab mat resilience is limited, however, by the maximum allowable static rail deflection. Nelson [3] reports a resonance frequency of 16 Hz for the resonance frequency of the coupled vehicle–track system in the case of the continuous floating slab in use at the Washington Metropolitan Area Transit System and resonance frequencies between 8 and 16 Hz for discontinuous slabs in several other rail transportation systems in the USA and Canada. Cui and Chew [5] discuss the design of the floating slab track of the Singapore Mass Rapid Transit system with a resonance frequency of 10 Hz. Schillemans [1] presents a study of the noise and vibration impact of the North–South high speed train connection through the city of Antwerp where a floating slab at 11 Hz is proposed for a tunnel in close proximity of building foundations.

The working principle of the floating slab track [2] or under ballast mats [6] is usually demonstrated by considering the transmissibility of a single degree of freedom system. The design is based on more elaborate models, that typically involve a continuous track model, where the rails and the concrete slab are modelled as beams with an infinite length and the rail pads and slab mats are represented by locally reacting vertical springs. Jones [7,8] uses such a two-dimensional track model, coupled to a three-dimensional layered half-space model for the soil, to study the effectiveness of anti-vibration systems. At the track–soil interface, a uniform distribution of the soil tractions is assumed. Nelson [3] and Nelson et al. [9] study the performance of ballast mats and floating slabs by means of a similar two-dimensional track model, which is coupled to a soil model that is based on a lumped parameter model of a foundation on a halfspace.

A large number of authors have recently presented similar track models. Sheng et al. [10,11] couple an infinite layered beam model for the track to a layered half-space model of the soil, using the Haskell–Thomson transfer matrices for the soil. Sheng et al. [12,13] also coupled a train model to the track and indicate that when the train speed is relatively low compared to the wave velocities in the soil, the dynamic component of the axle loads determines the vibration levels in the free field. Kaynia et al. [14] and Madshus and Kaynia [15] model the track by means of beam elements and calculate the impedance of the coupled track–soil system by means of the disc Green's functions for a horizontally layered half-space. Auersch [16] has coupled a finite element model for a finite track part to a boundary element model for the soil. This model has been used to calculate the track compliance that is subsequently used in the solution of the vehicle–track interaction problem. Metrikine et al. [17] study the stability of a moving train bogie by means of a two degree of freedom model for the bogie, which is coupled to a beam of infinite length for the track and a homogeneous half-space model for the soil, following an approach proposed by Metrikine and Popp [18].

Other models for dynamic track–soil interaction have been proposed by Andersen and Nielsen [19] who apply a boundary element method for the steady-state response of an elastic medium in a moving frame of reference. Ekevid and Wiberg [20] combine the finite element method and the scaled boundary element method for the quasi-static response of the coupled track–soil system.

Within the frame of the present paper, a three-dimensional numerical model [21] is applied to study the effectiveness of a floating slab for the control of ground-borne vibrations induced by railway traffic. The focus is on the influence of the dynamic track–soil interaction on the wave radiation by a dynamic point load on the track. The numerical model accounts for the dynamic interaction between the train, the track and the soil, as required for the calculation of the dynamic axle loads, which are the major source of ground-borne vibrations when the train speed is low compared to the wave velocities in the soil. The track is modelled by means of beams with an infinite length, while the soil is modelled as a horizontally layered elastic half-space. The soil impedance is calculated by means of the boundary element method, based on the Green's functions of a horizontally layered half-space. The model has been validated by means of several experiments that have been

performed at the occasion of the homologation tests of the new HST track on the line L2 between Brussels and Köln [21].

The outline of the paper is as follows. First, the general equations that govern the track–soil interaction are formulated for the case of a floating slab track. The effectiveness of the floating slab is studied by comparing with the performance of an ordinary (unisolated) slab track for both the case of a soft and a stiff soil. The track impulse response is calculated in the frequency–wavenumber domain and interpreted by means of the dispersion curves of the bending waves in the slab and the Rayleigh waves in the soil. The response at the track–soil interface is used to compute the insertion loss in the frequency–wavenumber domain. These results show at which wavenumbers and frequencies the response is reduced by the presence of the slab mat. Next, the transfer functions between the track and the free field are studied in the frequency–wavenumber domain and in the frequency domain. Finally, the response in the free field is used to compute the insertion loss.

2. The equations of motion of the track–soil system

In this subsection, the equations of motion of the coupled track–soil system are solved for a vertical impulse load at a fixed position $\{x_S, 0, z_S\}^{\mathrm{T}}$ on the track. The track is assumed to be located at the surface of a horizontally layered half-space, with a geometry that is invariant in the longitudinal direction $\mathbf{e}_y$ (Fig. 2). In the following, the more general case of the floating slab track is considered, as the expressions for the unisolated slab track are easily derived from the latter.

Fig. 3 shows a model for a floating slab track, where resilient elements are incorporated under the rails and under the concrete slab. The rails are modelled as Euler–Bernoulli beams with a bending stiffness $E_r I_r$ and a mass $\rho_r A_r$ per unit length. The rail displacements are denoted as $u_{r1}(y,t)$ and $u_{r2}(y,t)$. The positions of the rail are determined by l_1 and l_2.

The rail pads are modelled as continuous spring–damper connections. The rail pad stiffness k_{rp} and damping coefficient c_{rp} of a single rail pad are used to calculate an equivalent stiffness $\overline{k}_{rp} = k_{rp}/d$ and damping coefficient $\overline{c}_{rp} = c_{rp}/d$ in the continuous model, where d is the distance between the pads.

The concrete slab is assumed to be rigid in the plane of its cross section and modelled as a beam, accounting for both bending and torsional deformations. The width of the slab is denoted as $2B$ and the

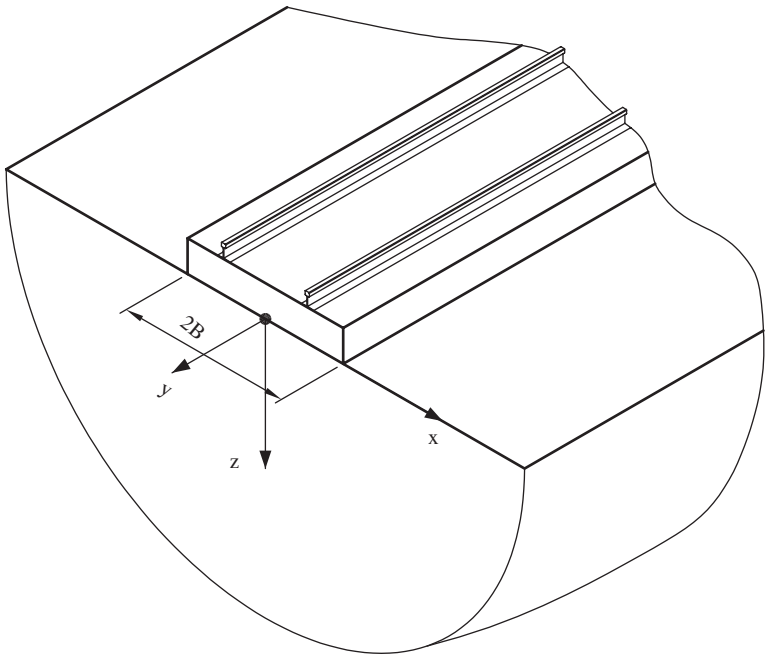

Fig. 2. Problem geometry.

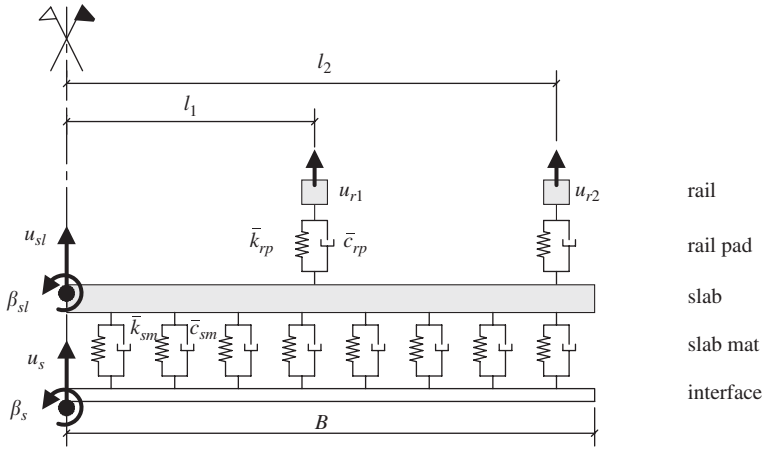

Fig. 3. Cross section of a numerical model for a floating slab.

height of the slab as h_{sl}. These geometric properties and the density ρ_{sl}, the Young's modulus E_{sl} and the shear modulus G_{sl} are used to calculate the mass per unit length $\rho_{\mathrm{sl}}A_{\mathrm{sl}} = \rho_{\mathrm{sl}}2Bh_{\mathrm{sl}}$, the bending stiffness $E_{\mathrm{sl}}I_{\mathrm{sl}} = E_{\mathrm{sl}}2Bh_{\mathrm{sl}}^3/12$, the mass moment of inertia $\rho_{\mathrm{sl}}I_{\mathrm{sl},t} = \rho_{\mathrm{sl}}2B^3h/3$ and the torsional stiffness $G_{\mathrm{sl}}C_{\mathrm{sl}} = G_{\mathrm{sl}}2Bh^3/3$ of the slab.

The slab mat is assumed to act as a set of distributed, independent linear springs and dampers, with a vertical stiffness K_{sm} [N/m^3]. The total vertical stiffness over the track width $2B$ is denoted as $\overline{k}_{sm}$ [N/m^2] and equal to $2BK_{sm}$. When viscous damping in the slab mat is accounted for, the dynamic impedance of the slab mat in the frequency domain equals $\overline{k}_{sm} + \mathrm{i}\omega\overline{c}_{sm}$.

The track–soil interface is assumed to be rigid in the plane of the track cross section. The vertical displacements $u_{sz}(x, y, t)$ at the track–soil interface Σ are therefore determined by the the vertical displacement $u_s(y, t)$ at the centre of the track–soil interface and the rotation $\beta_s(y, t)$ about this centre:

$$u_{sz}(x, y, t) = u_s(y, t) + \beta_s(y, t)x = \boldsymbol{\phi}_t(x)\boldsymbol{\alpha}(y, t) \quad \text{on } \Sigma, \tag{1}$$

where $\boldsymbol{\phi}_t(x)$ is the vector $\{1, x\}$ that collects the displacement modes of the cross section, while the vector $\boldsymbol{\alpha}(y, t)$ collects the displacement $u_s(y, t)$ and the rotation $\beta_s(y, t)$, which can be interpreted as generalised degrees of freedom.

The invariance of the geometry with respect to the longitudinal coordinate y allows a Fourier transformation of the coordinate y to the wavenumber k_y. This results in a solution procedure in the frequency–wavenumber domain, where the equations of motion of the coupled track–soil system can be written in the following general form:

$$[\tilde{\mathbf{K}}_{\mathrm{tr}} + \tilde{\mathbf{K}}_s]\tilde{\mathbf{u}}_{\mathrm{tr}} = \tilde{\mathbf{f}}_{\mathrm{tr}}, \tag{2}$$

$\tilde{\mathbf{K}}_{\mathrm{tr}}$ and $\tilde{\mathbf{K}}_s$ represent the track and the soil impedance matrices, respectively, while $\tilde{\mathbf{u}}_{\mathrm{tr}}$ is the track displacement vector and $\tilde{\mathbf{f}}_{\mathrm{tr}}$ is the force vector applied to the track. A tilde above a variable denotes its representation in the frequency–wavenumber domain, so that the arguments k_y and ω are omitted. The solution procedure has been originally proposed by Aubry et al. [22] and Clouteau et al. [23] to study the interaction of an infinite beam with a horizontally layered elastic half-space in the frequency–wavenumber domain.

The track displacement vector $\tilde{\mathbf{u}}_{\mathrm{tr}}$ collects the track displacements and the generalized degrees of freedom $\tilde{\boldsymbol{\alpha}}$ of the track–soil interface Σ. In the present case of a floating slab track, the vector $\tilde{\mathbf{u}}_{\mathrm{tr}}$ equals $\{\tilde{u}_{r1}, \tilde{u}_{r2}, \tilde{u}_{\mathrm{sl}}, \tilde{\beta}_{\mathrm{sl}}, \tilde{u}_s, \tilde{\beta}_s\}^{\mathrm{T}}$. The track force vector $\tilde{\mathbf{f}}_{\mathrm{tr}}$ contains the forces applied at both rails and is equal to $\{\tilde{f}_{r1}, \tilde{f}_{r2}, 0, 0, 0, 0\}^{\mathrm{T}}$.

The track impedance matrix $\tilde{\mathbf{K}}_{\mathrm{tr}}$ in the equations of motion (2) of the coupled track–soil system is

$$\tilde{\mathbf{K}}_{\mathrm{tr}} = \begin{bmatrix} \tilde{K}_r + \tilde{K}_{rp} & 0 & -\tilde{K}_{rp} & -\tilde{K}_{rp} l_1 & 0 & 0 \\ 0 & \tilde{K}_r + \tilde{K}_{rp} & -\tilde{K}_{rp} & -\tilde{K}_{rp} l_2 & 0 & 0 \\ -\tilde{K}_{rp} & -\tilde{K}_{rp} & \tilde{K}_{\mathrm{sl},b} + 2\tilde{K}_{rp} + \tilde{K}_{sm} & \tilde{K}_{rp}(l_1 + l_2) & -\tilde{K}_{sm} & 0 \\ -\tilde{K}_{rp} l_1 & -\tilde{K}_{rp} l_2 & \tilde{K}_{rp}(l_1 + l_2) & \tilde{K}_{\mathrm{sl},t} + \tilde{K}_{rp}(l_1^2 + l_2^2) + \tilde{K}_{sm} \frac{B^2}{3} & 0 & -\tilde{K}_{sm} \frac{B^2}{3} \\ 0 & 0 & -\tilde{K}_{sm} & 0 & \tilde{K}_{sm} & 0 \\ 0 & 0 & 0 & -\tilde{K}_{sm} \frac{B^2}{3} & 0 & \tilde{K}_{sm} \frac{B^2}{3} \end{bmatrix}, \quad (3)$$

where $\tilde{K}_r$ denotes the rail impedance $E_r I_r k_y^4 - \rho_r A_r \omega^2$ in the frequency–wavenumber domain and $\tilde{K}_{rp}$ is the dynamic stiffness $\overline{k}_{rp} + \mathrm{i}\omega\overline{c}_{rp}$ of the rail pads. $\tilde{K}_{\mathrm{sl},b} = E_{\mathrm{sl}} I_{\mathrm{sl}} k_y^4 - \rho_{\mathrm{sl}} A_{\mathrm{sl}} \omega^2$ and $\tilde{K}_{\mathrm{sl},t} = G_{\mathrm{sl}} C_{\mathrm{sl}} k_y^2 - \rho_{\mathrm{sl}} I_{\mathrm{sl},t} \omega^2$ are the slab bending and torsional impedance, respectively. The dynamic stiffness $\tilde{K}_{sm}$ of the slab mat in the vertical direction is equal to $\overline{k}_{sm} + \mathrm{i}\omega\overline{c}_{sm}$. The rotational impedance equals $\tilde{K}_{sm} b^2/3$.

In the case of the unisolated slab track, no distinction is made between the degrees of freedom $\tilde{u}_{\mathrm{sl}}$ and $\tilde{\beta}_{\mathrm{sl}}$ that describe the vertical slab response and the degrees of freedom $\tilde{u}_s$ and $\tilde{\beta}_s$ that describe the vertical response at the interface between the track and the soil. The track displacement vector $\tilde{\mathbf{u}}_{\mathrm{tr}}$ in this case is $\{\tilde{u}_{r1}, \tilde{u}_{r2}, \tilde{u}_{\mathrm{sl}}, \tilde{\beta}_{\mathrm{sl}}\}^{\mathrm{T}}$ and the track impedance matrix $\tilde{\mathbf{K}}_{\mathrm{tr}}$ is obtained by omitting the rows and columns in Eq. (3) that correspond to the degrees of freedom $\tilde{u}_s$ and $\tilde{\beta}_s$ and omitting the contribution related to $\tilde{K}_{sm}$ in the remaining elements.

The weak formulation of the vertical equilibrium at the track–soil interface Σ allows the calculation of the soil impedance matrix $\tilde{\mathbf{K}}_s$ in Eq. (2):

$$\tilde{K}_{sij}(k_y, \omega) = \int_{\Sigma} \phi_{ti} \tilde{t}_{sz}(\mathbf{u}_{sc}(\phi_{tj}))\, \mathrm{d}\Gamma, \quad (4)$$

where $\mathbf{u}_{sc}(\phi_{tj})$ is the wavefield in the soil due to an imposed displacement ϕ_{tj} at the track–soil interface Σ in the frequency–wavenumber domain. $\tilde{t}_{sz}(\mathbf{u}_{sc}(\phi_{tj}))$ is the vertical component of the soil tractions $\tilde{\mathbf{t}}_s = \tilde{\boldsymbol{\sigma}}_s \mathbf{n}$ on a boundary with a unit outward normal $\mathbf{n}$ due to this scattered wavefield $\mathbf{u}_{sc}(\phi_{tj})$. In the present case, the soil impedance matrix is equal to

$$\tilde{\mathbf{K}}_s = \begin{bmatrix} 0 & 0 & 0 & 0 & 0 & 0 \\ 0 & 0 & 0 & 0 & 0 & 0 \\ 0 & 0 & 0 & 0 & 0 & 0 \\ 0 & 0 & 0 & 0 & 0 & 0 \\ 0 & 0 & 0 & 0 & \tilde{K}_{s11} & 0 \\ 0 & 0 & 0 & 0 & 0 & \tilde{K}_{s22} \end{bmatrix}. \quad (5)$$

A boundary element method is used to calculate the soil tractions $\tilde{t}_{sz}(\mathbf{u}_{sc}(\phi_{tj}))$ at the track–soil interface, assuming that the track is located at the soil's surface [22,24]. The boundary element formulation is based on the boundary integral equations in the frequency–wavenumber domain, using the Green's functions of a horizontally layered soil [25–27]. Each soil layer is characterized by its thickness d, the elastic constants E and ν or the longitudinal and transversal wave velocities C_p and C_s, the material density ρ and a material damping ratio β_p and β_s in Eq. (2) that governs the volumetric and deviatoric deformation, respectively.

The solution of the track–soil interaction provides the soil displacements $\{\tilde{u}_s, \tilde{\beta}_s\}^{\mathrm{T}}$ at the track–soil interface Σ, which allow the computation of the soil tractions $\tilde{t}_{sz}(x, k_y, z = 0, \omega)$ at this interface:

$$\tilde{t}_{sz}(x, k_y, z = 0, \omega) = \tilde{\mathbf{t}}_{sz}(\mathbf{u}_{sc}(\boldsymbol{\phi}_t))\tilde{\boldsymbol{\alpha}}, \quad (6)$$

where $\tilde{\mathbf{t}}_{sz}(\mathbf{u}_{sc}(\boldsymbol{\phi}_t))$ collects the vertical component of the soil tractions due to the scattered wavefields in the soil.

The dynamic reciprocity theorem is used for the calculation of the track–soil transfer function $\tilde{h}_{zi}(x, k_y, z, \omega)$:

$$\tilde{h}_{zi}(x, k_y, z, \omega) = \int_{\Sigma} \tilde{u}_{zi}^{G}(x - x', k_y, z, \omega) \tilde{t}_{sz}(x', k_y, z' = 0, \omega)\, \mathrm{d}\Gamma \quad (7)$$

where $\tilde{u}^G_{zi}(x,k_y,z,\omega)$ is the representation in the frequency–wavenumber domain of the Green's function $u^G_{zi}(x,y,z,t)$, that represents the displacement in the direction $\mathbf{e}_i$ at a time t in a point $\{x,y,z\}^T$ due to an impulse load $\delta(t)$ in the vertical direction $\mathbf{e}_z$ at the origin of the frame of reference.

3. The track response

3.1. Dynamic properties of the track and the soil

In the following, the effectiveness of the floating slab track will be investigated for two different cases, where a track is coupled to a homogeneous elastic half-space with different soil properties.

The track is composed of two UIC60 rails with a bending stiffness $E_rI_r = 6.45 \times 10^6\,\mathrm{Nm}^2$ and a mass per unit length $\rho_rA_r = 60.3\,\mathrm{kg/m}$ for each rail. The rail pads have a stiffness $k_{rp} = 213.2 \times 10^6\,\mathrm{N/m}$ and a damping $c_{rp} = 14.8 \times 10^3\,\mathrm{Ns/m}$. A distance $d = 0.6\,\mathrm{m}$ between the rail pads is used to calculate the equivalent stiffness $\overline{k}_{rp} = k_{rp}/d$ and damping coefficient $\overline{c}_{rp} = c_{rp}/d$ in the continuous model. The concrete slab has a density $\rho_{\mathrm{sl}} = 2500\,\mathrm{kg/m}^3$, a Young's modulus $E_{\mathrm{sl}} = 30000\,\mathrm{N/mm}^2$ and a shear modulus $G_{\mathrm{sl}} = 11000\,\mathrm{N/mm}^2$. The width of the slab $2B$ equals 2.5 m and the height $h_{\mathrm{sl}} = 0.55\,\mathrm{m}$. In the case of the floating slab, a slab mat with a stiffness $K_{sm} = 15 \times 10^6\,\mathrm{N/m}^3$ and a damping coefficient $C_{sm} = 30 \times 10^3\,\mathrm{Ns/m}^3$ is considered.

The track is assumed to be located at the surface of a homogeneous half-space that represents the soil. In a first case, a homogeneous half-space with a shear wave velocity $C_s = 150\,\mathrm{m/s}$ and a dilatational wave velocity $C_p = 300\,\mathrm{m/s}$ is considered. The soil hysteretic material damping ratio β equals 0.025 in both shear and volumetric deformation. The phase velocity C_r of the Rayleigh waves is equal to 140 m/s in this case and is smaller than the phase velocity of the bending waves in the track in the frequency range of interest. This is therefore referred to as the case of the soft soil. In the second case, the Young's modulus of the soil is increased by a factor of 16, which results in a shear wave velocity $C_s = 600\,\mathrm{m/s}$ and a dilatational wave velocity $C_p = 1200\,\mathrm{m/s}$. This is the case of the stiff soil, as the Rayleigh phase velocity is now higher than the phase velocity of the bending waves.

3.2. The track impulse response in the frequency–wavenumber domain

The track impulse response in the frequency–wavenumber domain is found from the solution of the track–soil interaction equation (2). The impulse is applied at the track centre, so that the same load $\tilde{f}_{r1} = \tilde{f}_{r2} = 0.5$ is applied at both rails. Torsional waves in the slab are not excited.

Fig. 4a shows the rail impulse response as a function of the frequency $\omega/2\pi$ and the dimensionless wavenumber $\overline{k}_y$ in the case of the unisolated track on the soft soil. The shear wave velocity C_s of the homogeneous half-space has been used to define the dimensionless wavenumber $\overline{k}_y$ as k_yC_s/ω or, alternatively, as the ratio of C_s and the phase velocity C_y of the waves. Superimposed on this figure are the dispersion curve $\overline{k}_r = C_s/C_r$ of a Rayleigh wave in the y-direction and the dispersion curve $\overline{k}_b = C_s/C_b$ of a bending wave in the slab with a phase velocity C_b:

$$C_b = \sqrt[4]{\frac{E_{\mathrm{sl}}I_{\mathrm{sl}}}{\rho_{\mathrm{sl}}A_{\mathrm{sl}}}\omega^2}. \tag{8}$$

The Rayleigh wave dispersion curve corresponds to a horizontal line at $\overline{k}_y = 1.073$, due to the non-dispersive character of the Rayleigh wave in a homogeneous halfspace.

A local maximum of the rail response (Fig. 4a) is found near the point where the dispersion curve of the bending wave intersects the dispersion curve of the Rayleigh wave. The intersection occurs at a frequency f_{ts}:

$$f_{\mathrm{ts}} = \frac{1}{2\pi}C_r^2\sqrt{\frac{\rho_{\mathrm{sl}}A_{\mathrm{sl}}}{E_{\mathrm{sl}}I_{\mathrm{sl}}}} \tag{9}$$

which equals approximately 6 Hz in the present case. Sheng et al. [28] have discussed the crucial role of this frequency of intersection in the dynamic behaviour of the coupled track–soil system for the case of a moving harmonic or quasi-static load.

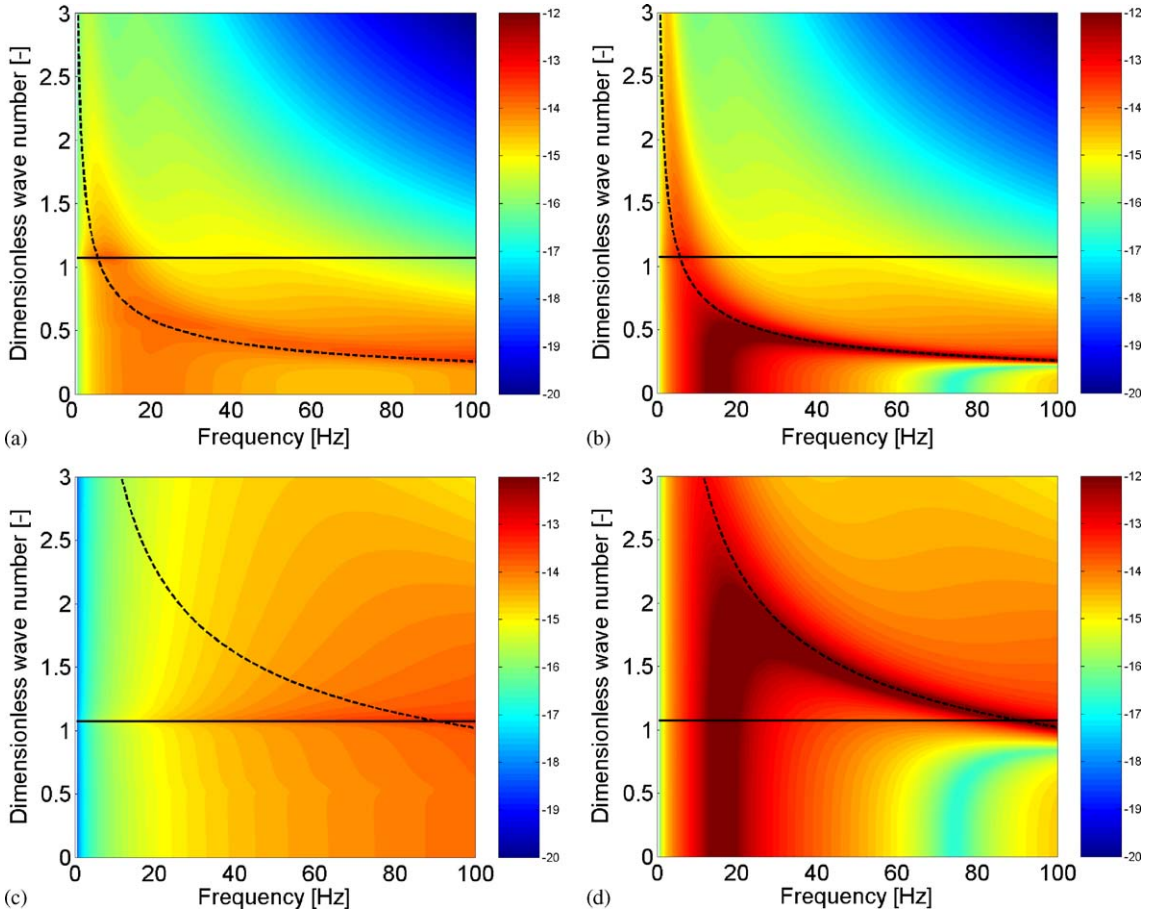

Fig. 4. Logarithm of the modulus of the rail displacement, multiplied by the circular frequency ω, in the frequency–wavenumber domain for (a) the unisolated track on soft soil, (b) the isolated track on soft soil, (c) the unisolated track on stiff soil, and (d) the isolated track on stiff soil. Superimposed on these figures are the dispersion curve of a Rayleigh wave in the y-direction (solid line) and the dispersion curve of the bending wave in the free slab (dashed line).

At higher frequencies, maxima are found along the dispersion curve of the track bending waves. As $\overline{k}_b$ is smaller than $\overline{k}_r$ in this frequency range, these maxima correspond to waves with a wavelength that is larger than the Rayleigh wavelength in the soil.

Fig. 4b shows the response of the isolated track. If the soil flexibility is disregarded, and the track is modelled as a beam on elastic foundation, a cut-on frequency of the bending waves occurs at the resonance frequency of the rigid track on the resilient slab mat:

$$f_{\mathrm{co}} = \frac{1}{2\pi}\sqrt{\frac{\overline{k}_{sm}}{\rho_{\mathrm{sl}} A_{\mathrm{sl}}}}, \tag{10}$$

which equals 16.3 Hz in the present case. At higher frequencies, the dispersion curve of the bending waves in the beam on elastic foundation tends towards the dispersion curve of the bending waves in the free beam. Fig. 4b shows a clear maximum for the rail response near this cut-on frequency and a zero dimensionless wavenumber. The peak response occurs at a frequency that is slightly lower than the computed value of 16.3 Hz due to the additional flexibility provided by the coupling of the track to the soil. The peak response is much larger than the response near the intersection of the dispersion curve of the Rayleigh wave in the y-direction and the track bending wave. At frequencies higher than the cut-on frequency, the maxima follow the dispersion curve of the slab bending waves. Compared to the case of the unisolated track, the maxima are

far more pronounced. This is due to the fact that, at frequencies higher than the cut-on frequency, the slab decouples from the soil and moves freely upon excitation. In the unisolated case, however, the coupling of the slab with the soil provides a strong damping mechanism by the radiation of waves and material damping in the soil.

Fig. 4c and d show similar results for the track on the stiff soil. The dispersion curve of the bending waves in the track is now found at dimensionless wavenumbers that are four times higher, as the shear wave velocity C_s of the stiff half-space is used to calculate the dimensionless wavenumber $\overline{k}_b = C_s/C_b$. According to Eq. (9), the frequency f_{ts} where the dispersion curve of the track bending wave and the Rayleigh wave intersect, and where a maximum rail response is found for the unisolated track, is multiplied by a factor of 16 or equal to 92 Hz (Fig. 4c).

At frequencies that are lower than f_{ts}, the maxima of the rail response do not occur near the dispersion curve of the bending waves, but near the dispersion curve of the Rayleigh wave. In the case of the isolated track (Fig. 4d), the maxima occur near the dispersion curve of the beam on elastic foundation. In the frequency range between f_{co} and f_{ts}, these maxima correspond to waves with a wavelength that is smaller than the Rayleigh wavelength in the soil.

Fig. 5 shows the impulse response at the interface between the track and the soil in the frequency–wavenumber domain. Compared to the response of the rail (Fig. 4), the response is more concentrated at dimensionless wavenumbers that are smaller than $\overline{k}_r$ and $\overline{k}_b$. Whereas the rail response in the

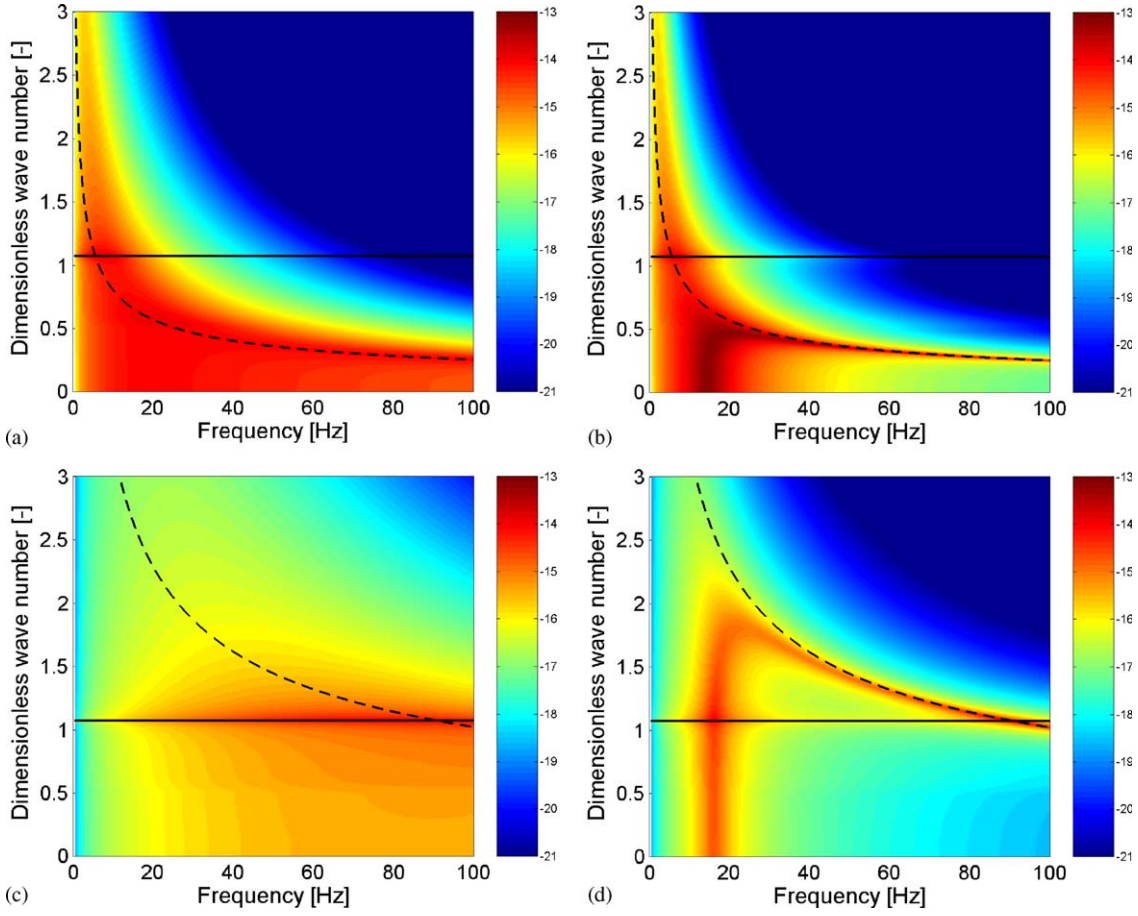

Fig. 5. Logarithm of the modulus of the displacement at the track-soil interface, multiplied by the circular frequency ω, in the frequency–wavenumber domain for (a) the unisolated track on soft soil, (b) the isolated track on soft soil, (c) the unisolated track on stiff soil, and (d) the isolated track on stiff soil. Superimposed on these figures are the dispersion curve of a Rayleigh wave in the y-direction (solid line) and the dispersion curve of the bending wave in the free slab (dashed line).

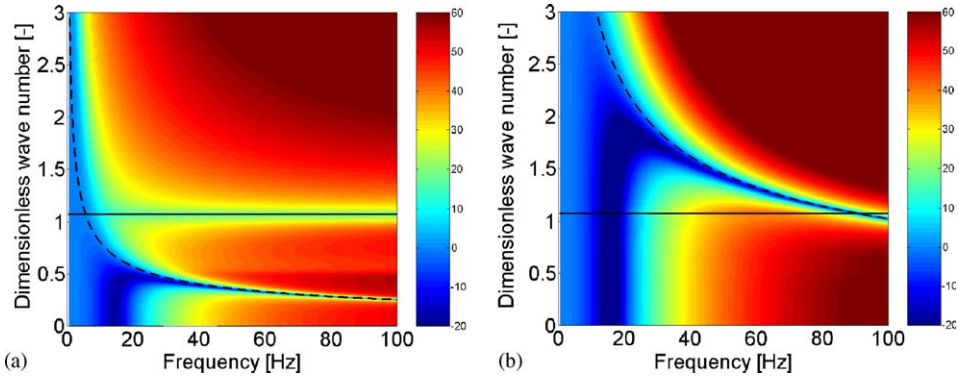

Fig. 6. Insertion loss at the track–soil interface in the frequency–wavenumber domain for the floating slab on (a) the soft soil and (b) the stiff soil. Superimposed on these figures are the dispersion curve of a Rayleigh wave in the y-direction (solid line) and the dispersion curve of the bending wave in the free slab (dashed line).

case of the isolated track (Figs. 4b and d) shows a single maximum near $\overline{k}_r$, a small local maximum is now also observed near $\overline{k}_r$ (Figs. 5b and d).

3.3. The insertion loss at the track–soil interface in the frequency–wavenumber domain

In order to verify for which frequencies and wavenumbers the response in the frequency–wavenumber domain has decreased due to the insertion of a flexible slab mat, the results in Fig. 5 are used to calculate the insertion loss IL from the ratio of the displacement at the track–soil interface of the unisolated and the isolated track:

$$\mathrm{IL} = 20\log\left(\frac{\tilde{u}_s^{\mathrm{uniso}}}{\tilde{u}_s^{\mathrm{iso}}}\right) \tag{11}$$

Positive values of the insertion loss correspond to a smaller response of the isolated track.

Fig. 6 shows the insertion loss for both cases. At frequencies below the slab resonance frequency, the insertion loss is negative and increases monotonically with the wavenumber $\overline{k}_y$, with a zero value at $\overline{k}_y \approx \overline{k}_b$. At frequencies well above the resonance frequency, the insertion loss is positive for all wavenumbers, except in a narrow region around $\overline{k}_b$, where it is negative. A small dip in the insertion loss is also observed near $\overline{k}_r$. At a fixed frequency higher than the slab resonance frequency, the presence of the slab mat therefore amplifies the response near $\overline{k}_b$, while it reduces the response at other wavenumbers. In the case of the soft soil (Fig. 6a), the stronger contribution near $\overline{k}_b$ is found in the wavenumber range between zero and $\overline{k}_r$, or at wavelengths that are larger than the Rayleigh wavelength λ_r. In the case of the stiff soil (Fig. 6b), the stronger contribution near $\overline{k}_b$ is found at wavenumbers larger than $\overline{k}_r$, or at wavelengths smaller than λ_r, in a frequency range between 30 and 90 Hz. In the following, it is shown how this affects the radiation of waves by a dynamic point load on the track and the reduction of the vibrations in the free field.

3.4. The track receptance

The frequency content of the track impulse response is found as the inverse Fourier transformation of the track displacement vector $\tilde{\mathbf{u}}_{\mathrm{tr}}$:

$$\hat{\mathbf{u}}_{\mathrm{tr}}(y,\omega) = \frac{1}{2\pi}\int_{-\infty}^{+\infty} \tilde{\mathbf{u}}_{\mathrm{tr}}(k_y,\omega)\exp(-\mathrm{i}k_y y)\,\mathrm{d}k_y. \tag{12}$$

The track receptance, or the response at the point $y = 0$ where the impulse load is applied, is found from an integration of the results shown in Figs. 4 and 5 along the k_y axis. Whereas all previous results in the frequency-wavenumber domain are shown upto a dimensionless wavenumber of 3, a much higher

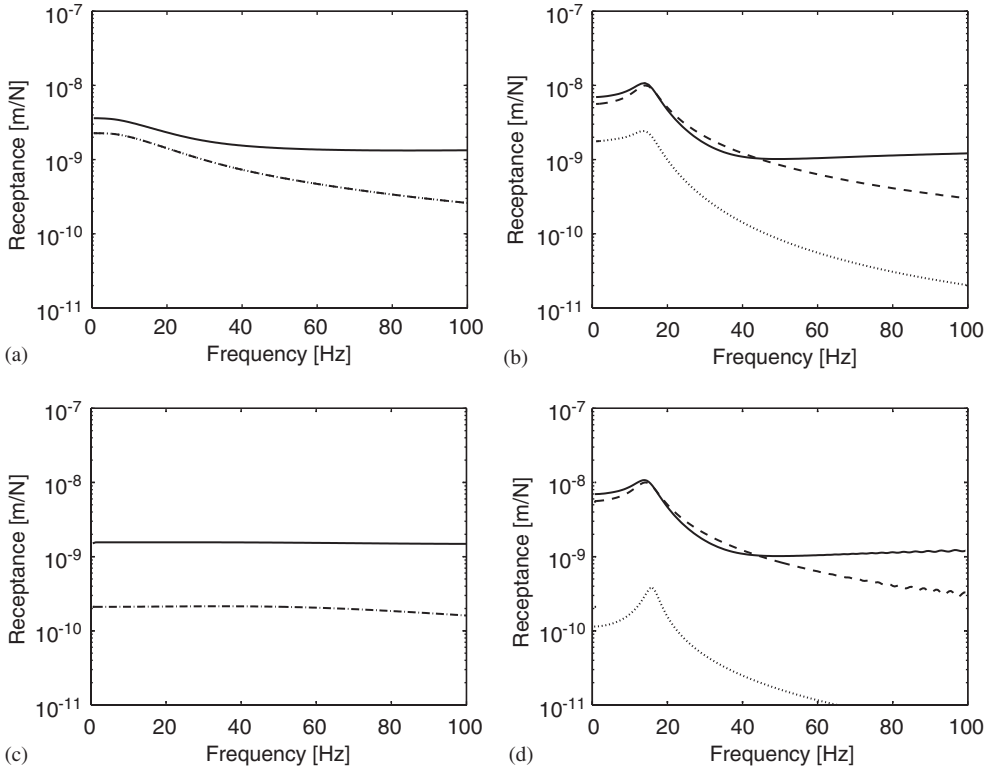

Fig. 7. The displacement of the rail (solid line), the slab (dashed line) and the track–soil interface (dotted line) for (a) the unisolated track on soft soil, (b) the isolated track on soft soil, (c) the unisolated track on stiff soil, and (d) the isolated track on stiff soil.

dimensionless wavenumber of $\overline{k}_y^{\max} = 1000$ has been considered for the inverse Fourier transformation from k_y to y.

Fig. 7 shows the track receptance for the isolated and unisolated track. In the case of the unisolated track, the slab displacement and the displacement at the track–soil interface coincide. At low frequencies, the flexibility of the mat results in a higher rail and slab response. The response at the track–soil interface is slightly smaller, as the softer support of the slab by the slab mat spreads the load over a larger area.

At the slab resonance frequency, the displacement of the rail, the slab and at the track–soil interface is much higher in the case of the isolated track. At higher frequencies, the presence of the slab mat significantly reduces the response at the track–soil interface. The response of the rail and the slab tend to a similar order of magnitude as in the case of the unisolated track.

When the results of the track on the soft and the stiff soil are compared, the larger stiffness importantly reduces the response at the track–soil interface. Furthermore, in the case of the unisolated track, the frequency dependence of the track response has changed importantly, due to the shift of the frequency of intersection f_{ts} in the frequency–wavenumber domain (Fig. 5).

3.5. The insertion loss at the track–soil interface in the frequency domain

The results in Fig. 7 have been used to calculate the insertion loss IL at the track–soil interface, defined as the ratio of the displacement at the point $y = 0$ without and with the slab mat. The results for the soft and the stiff soil show an IL with a similar tendency (see Fig. 8). At low frequencies, the IL is positive, as the introduction of the resilient mat spreads the load over a larger area and decreases the response at the point $y = 0$ of the track–soil interface. This effect is more pronounced for the floating slab on the stiff soil. At the slab resonance frequency, the response at the interface is much higher in the case of the floating slab and the IL is negative. At higher frequencies, the interface response is effectively reduced, with a

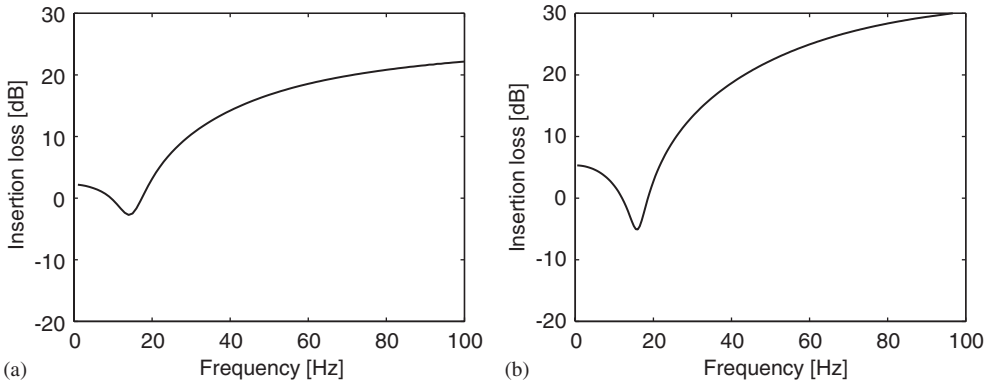

Fig. 8. Insertion loss at the track–soil interface for (a) the soft soil and (b) the stiff soil.

better performance for the floating slab on the stiff soil. In this case, the response in the frequency–wavenumber domain (Fig. 5d) is almost uniformly reduced in a dimensionless wavenumber range between 0 and $\overline{k}_r$, where the response is large. Similarly, the more uniform amplification of the response near the slab resonance frequency in this wavenumber range explains why the dip of the IL is more pronounced in the case of the stiff soil.

Although not shown on these figures, the better performance of the floating slab on the stiff soil occurs at the expense of a larger amplification of the rail response upto frequencies that are $\sqrt{2}$ times higher than the slab resonance frequency.

4. The free field impulse response

4.1. The track–soil transfer functions

The solution of the track–soil interaction equation (2) allows the calculation of the soil tractions at the track–soil interface by means of Eq. (6). The transfer function between the track and the free field in the frequency-wavenumber domain is computed by means of Eq. (7).

Fig. 9 shows the modulus of the free field velocity at $x = 8$ m in the frequency–wavenumber domain. In the present load case, only a single displacement mode contributes to the tractions in Eq. (6) and the transfer function is obtained as the product of the response at the track–soil interface (Fig. 5) and the integral of the product of the Green's function of the soil and the traction distribution. As only the first factor depends on the track characteristics, the insertion loss at the track–soil interface in the frequency wavenumber domain (Fig. 6) also determines the reduction of the track–soil transfer function in Fig. 9.

When the results in Figs. 5 and 9 are compared, it is observed that the contribution at wavenumbers higher than $\overline{k}_r$ is strongly reduced. Physically, this is explained by the fact that the waves at the interface with a dimensionless wavenumber larger than $\overline{k}_r$, or with a wavelength smaller than λ_r, cannot radiate Rayleigh waves that propagate into the free field. As a consequence, a large difference is observed between the results for the floating slab on the soft and the stiff soil, respectively. In the case of the soft soil, the contribution of waves with a wavenumber $\overline{k}_b$ smaller than $\overline{k}_r$ is amplified, and this amplification is clearly observed in the results for the free field velocity. In the case of the stiff soil, however, the contribution of waves with a wavenumber $\overline{k}_b$ larger than $\overline{k}_r$ is amplified in a frequency range between 30 and 90 Hz, and this amplification is effectively filtered by the soil.

4.2. The free field mobility

The frequency content of the displacements in the free field due to an impulse load on the track is calculated in a similar way as the track receptance by means of an inverse Fourier transform of the track-free

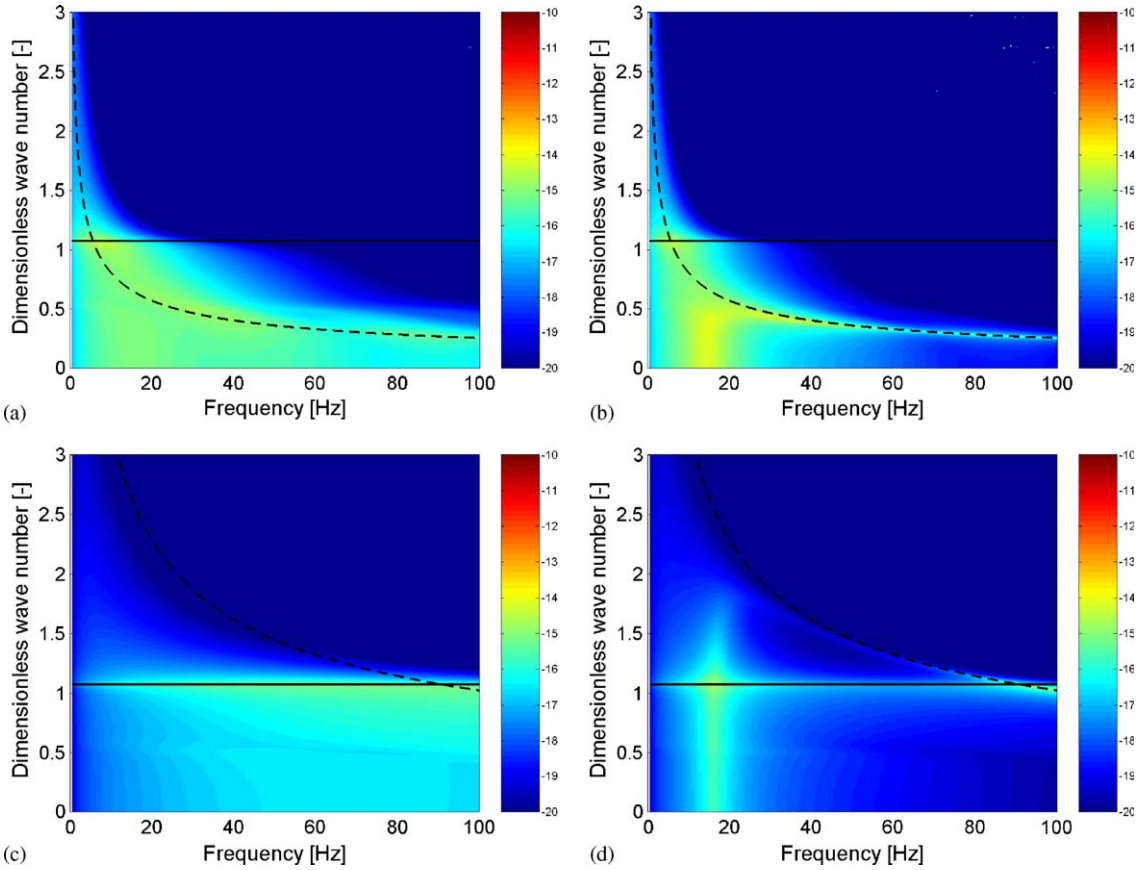

Fig. 9. Logarithm of the modulus of the vertical velocity at 8 m from the track, in the frequency–wavenumber domain for (a) the unisolated track on soft soil, (b) the isolated track on soft soil, (c) the unisolated track on stiff soil, and (d) the isolated track on stiff soil. Superimposed on these figures are the dispersion curve of a Rayleigh wave in the y-direction (solid line) and the dispersion curve of the bending wave in the free slab (dashed line).

field transfer functions:

$$\hat{h}_{zi}(x,y,z,\omega) = \frac{1}{2\pi}\int_{-\infty}^{+\infty} \tilde{h}_{zi}(x,k_y,z,\omega)\exp(-\mathrm{i}k_y y)\,\mathrm{d}k_y \tag{13}$$

The results in Fig. 9 have been used to calculate the free field velocity at $x = 8$ m and y equal to 0, 8 and 16 m (Fig. 10). In the case of the unisolated track on soft soil (Fig. 10a), the free field mobility decreases with increasing y and, therefore, with an increasing distance $r = \sqrt{x^2 + y^2}$ from the point on the track where the load is applied. The same holds for the isolated track (Fig. 10b), at frequencies below the slab resonance frequency. At higher frequencies between 30 and 50 Hz, however, a higher response is found at $y = 8$ m and $y = 16$ m. The non-uniform reduction of the response at the track–soil interface (Fig. 6a) in the dimensionless wavenumber range between 0 and $\overline{k}_r$ changes the radiation of waves by a dynamic point load on the track.

In the case of the stiff soil (Figs. 10c and d), this effect does not occur at frequencies between 30 and 60 Hz. In this frequency range, the response at the interface (Fig. 6b) is uniformly reduced in the dimensionless wavenumber range between 0 and $\overline{k}_r$.

In order to get a better view on the radiation of waves by a dynamic point load on the track, the free field displacements are computed in a large number of points on the track and in the free field. The computation has been performed by means of an efficient technique [29] that is based on the use of global shape functions for the representation of the soil tractions at the track–soil interface.

Fig. 11 compares the displacements of the track and in the free field due to a harmonic unit load at a frequency of 8 Hz on the unisolated and the isolated track for the case of the soft and the stiff soil. For both

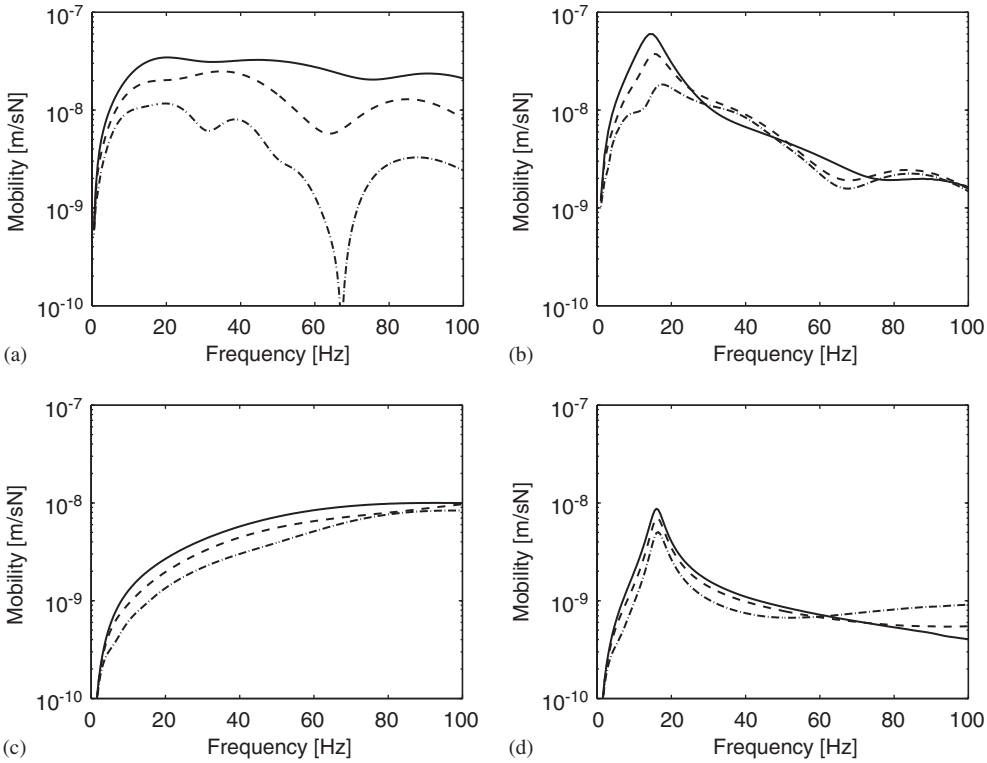

Fig. 10. Free field mobility at $x = 8\,\mathrm{m}$ and $y = 0\,\mathrm{m}$ (solid line), $y = 8\,\mathrm{m}$ (dashed line) and $y = 16\,\mathrm{m}$ (dashed-dotted line) for (a) the unisolated track on soft soil, (b) the isolated track on soft soil, (c) the unisolated track on stiff soil, and (d) the isolated track on stiff soil.

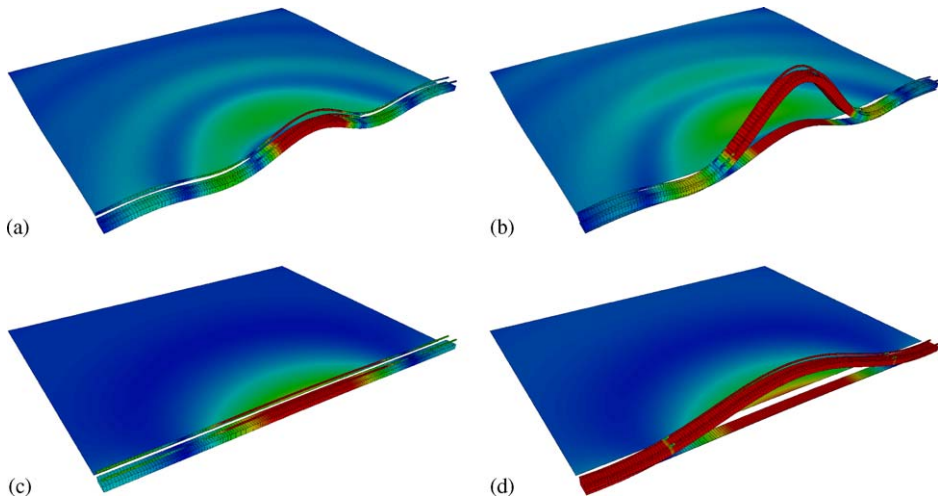

Fig. 11. The free field displacements due to a harmonic load at 8 Hz on the track for (a) the unisolated track on soft soil, (b) the isolated track on soft soil, (c) the unisolated track on stiff soil, and (d) the isolated track on stiff soil.

cases, the results for the unisolated and the isolated track are shown on the same scale. When the response of the unisolated and the isolated track are compared, it is observed that the displacements in the free field show a similar pattern, with a slightly larger response on a line perpendicular to the track. This is due to the dynamic amplification of the response near the slab resonance frequency. The displacements of the rail and the slab are clearly larger in the case of the isolated track due to the additional flexibility of the resilient mat.

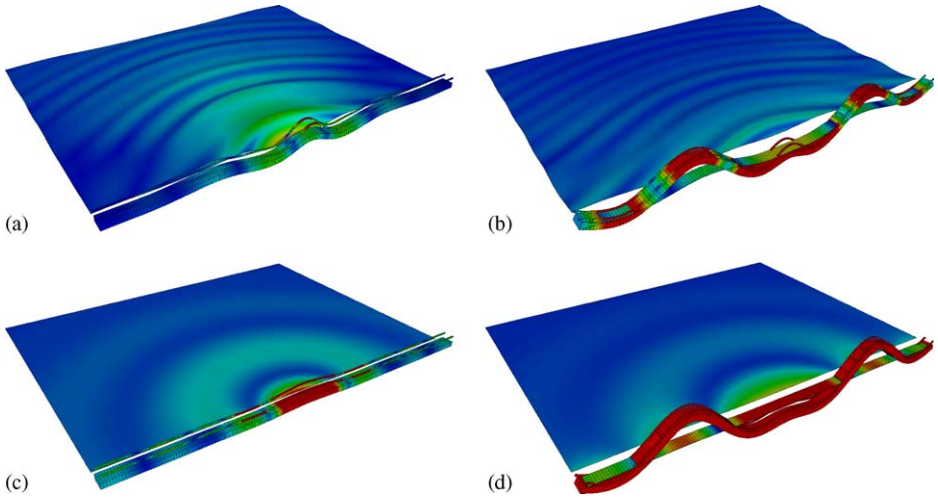

Fig. 12. The free field displacements due to a harmonic load at 32 Hz on the track for (a) the unisolated track on soft soil, (b) the isolated track on soft soil, (c) the unisolated track on stiff soil, and (d) the isolated track on stiff soil.

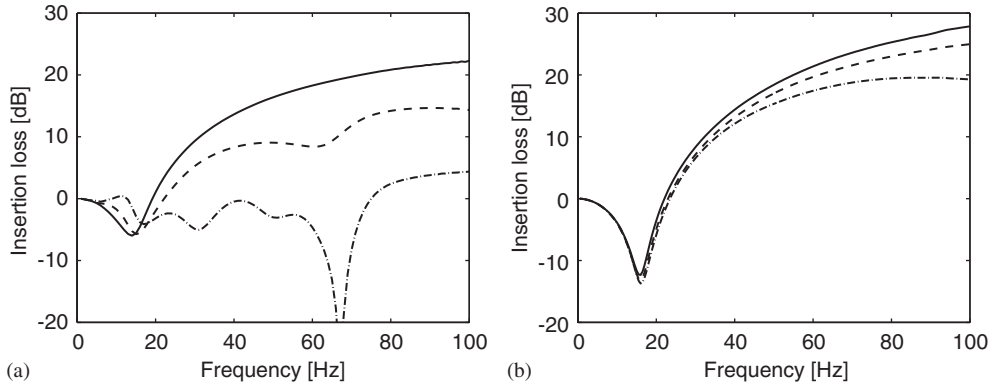

Fig. 13. Insertion loss for the floating slab at $x = 8$ m and $y = 0$ m (solid line), $y = 8$ m (dashed line) and $y = 16$ m (dashed-dotted line) for the case of (a) the soft soil and (b) the stiff soil.

Fig. 12 compares the track and the free field displacements due to a harmonic unit load at a frequency of 32 Hz, which is well above the slab resonance frequency. In the case of the soft soil, the presence of the resilient mat has completely changed the radiation of waves. Whereas in the unisolated case (Fig. 12a), large free field displacements are found due to the radiation of waves perpendicular to the track, this is no longer the case for the isolated track (Fig. 12b). The slab is clearly uncoupled from the soil and the bending waves in the uncoupled slab result in larger displacements along the track and an effective reduction of waves radiated perpendicular to the track. In the case of the isolated track on the stiff soil (Fig. 12d), the slab has uncoupled from the soil as well and a large amplification of the track response is observed as compared to the unisolated case (Fig. 12c). The free field displacements are radiated in a similar way as in the unisolated case, but with a much smaller amplitude.

The results in Fig. 10 have been used to compute the insertion loss for the free field response in Fig. 13. Whereas the results for the insertion loss at the track–soil interface (Fig. 8) show a positive value at low frequencies, due to the load spreading of the resilient slab, this is no longer the case for the insertion loss in the free field. A reduction of the free field vibrations is only achieved at frequencies sufficiently higher than the slab resonance frequency, at the expense of an increased response at lower frequencies. In the case of the soft soil (Fig. 13a), the insertion loss is high for the point at $y = 0$, but is much lower at $y = 8$ m and $y = 16$ m.

The effective reduction depends on the angle between the track and the line that connects the source on the track and the receiver in the free field. For a moving harmonic load, the response during the approach and the receding is less reduced than the peak response at the time where the source passes the receiver. In the case of the stiff soil (Fig. 13b), a rather uniform attenuation is obtained in the frequency range between 30 and 60 Hz. The floating slab on the stiff soil shows a better performance, at the expense of an increased response near the slab resonance frequency.

5. Conclusion

A numerical model for the prediction of railway induced vibrations has been applied to study the reduction of the free field vibrations by means of a floating slab track. The focus is on the influence of the dynamic track–soil interaction on the performance of the floating slab. Therefore, the reduction of the free field vibrations is investigated for a floating slab on a relatively soft soil and a stiff soil.

The longitudinal invariance of the track–soil system allows an efficient solution procedure in the frequency–wavenumber domain. The analysis of the track and free field response in the frequency–wavenumber domain shows how the response is not only amplified at the slab resonance frequency, as expected from a two-dimensional analysis, but also along the dispersion curve of the track bending waves. In the case of the soft soil, where the phase velocity of the bending waves in the track is higher than the Rayleigh wave velocity in the soil, this modifies the radiation of waves by a dynamic point load on the track. The resulting insertion loss for the free field response is relatively high for points on a line perpendicular to the track, but is much less for other points in the free field. In the case of the stiff soil, where the phase velocity of the bending waves in the track is lower, the radiation of waves remains relatively unaffected. The reduction of the free field response is similar for all points in the free field.

References

[1] L. Schillemans, Impact of sound and vibration of the north-south high-speed railway connection through the city of Antwerp, Belgium, *Journal of Sound and Vibration* 267 (2003) 637–649.
[2] G.P. Wilson, H.J. Saurenman, J.T. Nelson, Control of ground-borne noise and vibration, *Journal of Sound and Vibration* 87 (2) (1983) 339–350.
[3] J.T. Nelson, Recent developments in ground-borne noise and vibration control, *Journal of Sound and Vibration* 193 (1) (1996) 367–376.
[4] B. Hemsworth, Reducing groundborne vibrations: state of the art study, *Journal of Sound and Vibration* 231 (3) (2000) 703–709.
[5] F. Cui, C.H. Chew, The effectiveness of floating slab track system—Part I, receptance methods, *Applied Acoustics* 61 (2000) 441–453.
[6] R. Wettschureck, U.J. Kurze, Einfügungsdämmass von Unterschottermatten, *Acustica* 58 (1985) 177–182.
[7] C.J.C. Jones, Use of numerical-models to determine the effectiveness of anti-vibration systems for railways, *Proceedings of the Institution of Civil Engineers-Transport* 105 (1) (1994) 43–51.
[8] C.J.C. Jones, Ground-borne noise from new railway tunnels, *Proceedings of InterNoise '96*, 1996, pp. 421–426.
[9] J.T. Nelson, G.P. Wilson, Ground-borne noise and vibration control: a state-of-the-art perspective, *Proceedings of InterNoise '96*, 1996, pp. 1287–1292.
[10] X. Sheng, C.J.C. Jones, M. Petyt, Ground vibration generated by a harmonic load acting on a railway track, *Journal of Sound and Vibration* 225 (1) (1999) 3–28.
[11] X. Sheng, C.J.C. Jones, M. Petyt, Ground vibration generated by a load moving along a railway track, *Journal of Sound and Vibration* 228 (1) (1999) 129–156.
[12] X. Sheng, C.J.C. Jones, D.J. Thompson, A comparison of a theoretical model for quasi-statically and dynamically induced environmental vibration from trains with measurements, *Journal of Sound and Vibration* 267 (3) (2003) 621–635.
[13] X. Sheng, C.J.C. Jones, D.J. Thompson, A theoretical model for ground vibration from trains generated by vertical track irregularities, *Journal of Sound and Vibration* 272 (3–5) (2004) 937–965.
[14] A.M. Kaynia, C. Madshus, P. Zackrisson, Ground vibration from high speed trains: prediction and countermeasure, *Journal of Geotechnical and Geoenvironmental Engineering, Proceedings of the ASCE* 126 (6) (2000) 531–537.
[15] C. Madshus, A.M. Kaynia, High-speed railway lines on soft ground: dynamic behaviour at critical train speed, *Journal of Sound and Vibration* 231 (3) (2000) 689–701.
[16] L. Auersch, The excitation of ground vibration by rail traffic: theory of vehicle-track-soil interaction and measurements on high-speed lines, *Journal of Sound and Vibration* 284 (1–2) (2005) 103–132.
[17] A.V. Metrikine, S.N. Verichev, J. Blauwendraad, Stability of a two-mass oscillator moving on a beam supported by a visco-elastic half-space, *International Journal of Solids and Structures* 42 (2005) 1187–1207.

[18] A.V. Metrikine, K. Popp, Steady-state vibrations of an elastic beam on a visco-elastic layer under moving load, *Archive of Applied Mechanics* 70 (2000) 399–408.
[19] L. Andersen, S.R.K. Nielsen, Boundary element analysis of the steady-state response of an elastic half-space to a moving force on its surface, *Engineering Analysis with Boundary Elements* 27 (2003) 23–38.
[20] T. Ekevid, N.-E. Wiberg, Wave propagation related to high-speed train, A scaled boundary FE-approach for unbounded domains, *Computer Methods in Applied Mechanics and Engineering* 191 (2002) 3947–3964.
[21] G. Lombaert, G. Degrande, J. Kogut, S. François, The experimental validation of a numerical model for the prediction of railway induced vibrations, *Journal of Sound and Vibration*, 2006, in press, doi:10.1016/j.jsv.2006.03.048.
[22] D. Aubry, D. Clouteau, G. Bonnet, Modelling of wave propagation due to fixed or mobile dynamic sources, in: N. Chouw, G. Schmid (Eds.), *Workshop Wave '94*, *Wave propagation and Reduction of Vibrations*, Ruhr Universität Bochum, Germany, December 1994, pp. 109–121.
[23] D. Clouteau, G. Degrande, G. Lombaert, Numerical modelling of traffic induced vibrations, *Meccanica* 36 (4) (2001) 401–420.
[24] G. Lombaert, G. Degrande, D. Clouteau, Numerical modelling of free field traffic induced vibrations, *Soil Dynamics and Earthquake Engineering* 19 (7) (2000) 473–488.
[25] J.E. Luco, R.J. Apsel, On the Green's functions for a layered half-space, Part I, *Bulletin of the Seismological Society of America* 4 (1983) 909–929.
[26] F.C.P. de Barros, J.E. Luco, Moving Green's functions for a layered visco-elastic halfspace, Technical report, Department of Applied Mechanics and Engineering Sciences, University of California, San Diego, La Jolla, California, May 1992.
[27] E. Kausel, J.M. Roësset, Stiffness matrices for layered soils, *Bulletin of the Seismological Society of America* 71 (6) (1981) 1743–1761.
[28] X. Sheng, C.J.C. Jones, D.J. Thompson, A theoretical study of the influence of the track on train-induced ground vibration, *Journal of Sound and Vibration* 272 (3–5) (2004) 909–936.
[29] S. François, G. Lombaert, G. Degrande, Comparison between local and global shape functions in a boundary element method for the calculation of traffic induced vibrations, *Soil Dynamics and Earthquake Engineering* 25 (11) (2005) 839–856.